High Power Laser Science and Engineering, (2023), Vol. 11, e12, 9 pages.
doi:10.1017/hpl.2023.3

HIGH POWER LASER SCIENCE AND ENGINEERING

RESEARCH ARTICLE

2.1 μm, high-energy dissipative soliton resonance from a holmium-doped fiber laser system

Desheng Zhao[1,2,3], Bin Zhang[1,2,3], Xiran Zhu[1,2,3], Shuailin Liu[1,2,3], Li Jiang[1,2,3], Zhiyuan Dou[1,2,3], Linyong Yang[1,2,3], and Jing Hou[1,2,3]

[1] *College of Advanced Interdisciplinary Studies, National University of Defense Technology, Changsha, China*

[2] *Nanhu Laser Laboratory, National University of Defense Technology, Changsha, China*

[3] *Hunan Provincial Key Laboratory of High Energy Laser Technology, Changsha, China*

(Received 18 October 2022; revised 30 November 2022; accepted 28 December 2022)

Abstract

We propose a 2.1 μm high-energy dissipative soliton resonant (DSR) fiber laser system based on a mode-locked seed laser and dual-stage amplifiers. In the seed laser, the nonlinear amplifying loop mirror technique is employed to realize mode-locking. The utilization of an in-band pump scheme and long gain fiber enables effectively exciting 2.1 μm pulses. A section of ultra-high numerical aperture fiber (UHNAF) with normal dispersion and high nonlinearity and an output coupler with a large coupling ratio are used to achieve a high-energy DSR system. By optimizing the UHNAF length to 55 m, a 2103.7 nm, 88.1 nJ DSR laser with a 3-dB spectral bandwidth of 0.48 nm and a pulse width of 17.1 ns is obtained under a proper intracavity polarization state and pump power. The output power and conversion efficiency are 0.233 W and 4.57%, respectively, both an order of magnitude higher than those of previously reported holmium-doped DSR seed lasers. Thanks to the high output power and nanosecond pulse width of the seed laser, the average power of the DSR laser is linearly scaled up to 50.4 W via a dual-stage master oscillator power amplifier system. The 3-dB spectral bandwidth broadens slightly to 0.52 nm, and no distortion occurs in the amplified pulse waveform. The corresponding pulse energy reaches 19.1 μJ, which is the highest pulse energy in a holmium-doped mode-locked fiber laser system to the best of our knowledge. Such a 2.1 μm, high-energy DSR laser with relatively wide pulse width has prospective applications in mid-infrared nonlinear frequency conversion.

Keywords: dissipative soliton resonance; high pulse energy; holmium-doped fiber laser system; mode-locking

1. Introduction

Pulsed fiber lasers of 2.1 μm have gained widespread interest due to their inherent advantages in a range of application fields, including free-space communication, mid-infrared nonlinear frequency conversion and so on[1–4]. For example, in free-space communication, a high repetition frequency (~GHz) pulsed laser in the 2.1 μm band exhibits more reliable data transmission than a short-wave high repetition frequency pulsed laser in extremely dense smoke conditions[1]. For mid-infrared nonlinear frequency conversion, a high-energy pulsed laser source excited in the 2.1 μm band is well matched to pump $ZnGeP_2$ (ZGP) and $BaGa_4Se_7$ (BGSe) crystals[5,6]. In particular, the 2.1 μm high-energy pulsed laser source with wide pulse width (a few nanoseconds to tens of nanoseconds) has become the preferred pump source for ZGP optical parametric oscillators (OPOs). The replacement of a solid-state laser source with an efficient and reliable fiber laser source can reduce the system size, lower maintenance costs and enhance system robustness, which has been investigated by several research groups[7–9]. For example, a 2.108 μm high-energy nanosecond pulse from an all-fiber holmium-doped amplification system has been applied in ZGP-OPO and obtained a mid-infrared conversion efficiency of up to 59%[7]. By employing thulium-doped fiber (TDF)[10,11], thulium-holmium co-doped fiber (THDF)[12], holmium-doped fiber (HDF)[13,14], pulsed laser at wavelengths exceeding 2 μm have been achieved. Compared with TDF and THDF, HDF pumped by a 1950 nm laser

Correspondence to: Bin Zhang and Jing Hou, College of Advanced Interdisciplinary Studies, National University of Defense Technology, Changsha 410073, China. Email: nudtzhb@163.com (B. Zhang); houjing25@sina.com (J. Hou)

has higher lasing efficiency, especially in the emission range of 2050–2150 nm[15].

Thanks to the wave-free splitting feature of dissipative soliton resonant (DSR) lasers, a high-energy DSR pulse can be obtained by controlling the fiber laser intracavity parameters[16,17]. Also, since the formed DSR laser has a wide pulse width, scaling of the DSR power is enabled by using an all-fiber master oscillator power amplifier (MOPA) configuration without precise dispersion management, which reduces the complexity of building the experimental amplification system. In ytterbium-doped[18,19], erbium-doped[20,21] and thulium-doped[22] fiber laser systems, the generation and amplification of high-energy DSR lasers have been studied greatly. However, a high-power DSR laser system operating at the 2.1 μm waveband has not been reported yet. Wang and Wu[18] reported a 1056 nm, 0.25 μJ DSR laser from an ytterbium-doped nonlinear polarization rotation (NPR) fiber laser and they scaled the pulse energy of the DSR laser to 0.51 mJ by a dual-stage MOPA structure. For an erbium-doped fiber laser system, Mao *et al.*[20] achieved 1530 nm, 2 μJ DSR output from dual-stage amplifiers. For a TDF laser, Zheng *et al.*[22] obtained a 130.5 nJ DSR pulse centered at 1976 nm in a double-clad oscillator. By utilizing a three-stage MOPA system, the DSR pulse energy reaches 0.33 mJ. For a holmium-doped seed laser, Zhao *et al.*[23] obtained a 5.8 nJ DSR laser with a center wavelength of 2024 nm by using the nonlinear optical loop mirror (NOLM) technique. Li *et al.*[24] used a nonlinear amplifying loop mirror (NALM) to achieve 2075 nm, 2 nJ DSR generation in a figure-of-eight cavity. Different from DSR lasers operating at short wavelengths, lower gain as well as higher loss of optical fiber and devices makes it a challenge to achieve wavelengths beyond 2.1 μm high-energy dissipative soliton resonance for mode-locked fiber lasers. Although DSR pulses can be obtained using the NPR technique, the polarization dependence of NPR results in the NPR-based fiber laser having poor environmental stability. In contrast, the polarization independence of the NALM/NOLM allows for a more robust system. Compared with the NOLM technique, the NALM technique can induce a larger nonlinear phase shift difference and thus reduce the mode-locking threshold, which is beneficial to the formation of long-wavelength DSR lasers. So far, the highest pulse energy achieved in the reported holmium-doped DSR mode-locked fiber laser is 26.5 nJ[25], and the operating wavelength of the reported DSR fiber laser is still limited to below 2.1 μm. The performance of holmium-doped mode-locked fiber lasers is not fully explored and there is room for improvement, especially in the generation and amplification of 2.1 μm mode-locked pulses. Further, designing a holmium-doped mode-locked fiber laser system to obtain a high-energy pulsed laser with a wide pulse width can satisfy the demand for mid-infrared nonlinear frequency conversion applications.

In this paper, a high-energy DSR HDF laser system is proposed. The DSR fiber laser system consists of a mode-locked seed laser and dual-stage amplifiers. Mode-locking is achieved by utilizing the NALM technique. Under a suitable intracavity polarization state and pump power, a 0.233 W, 17.1 ns square-wave DSR pulse with a center wavelength of 2103.7 nm is emitted from the mode-locked seed laser. The 3-dB spectral bandwidth is 0.48 nm. The pulse energy and conversion efficiency reach 88.1 nJ and 4.57%, respectively. The output power and conversion efficiency are improved by an order of magnitude compared to the reported holmium-doped DSR seed lasers. After amplification by the dual-stage amplifiers, the average power of the DSR pulse is scaled to 50.4 W. The corresponding pulse energy reaches 19.1 μJ, which represents the highest pulse energy for DSR lasers operating in the 2.1 μm waveband.

2. Experimental setup

The experimental layout of the mode-locked seed laser is presented in Figure 1. The cavity is designed as a figure-of-eight cavity structure, which is composed of a NALM ring and a unidirectional ring (UR). In the NALM ring, an in-band pump scheme is achieved by using a 1950 nm continuous wave (CW) TDF laser (TDFL 1) to pump the gain fiber. The maximum output power of TDFL 1 is 5.1 W. A 1950/2100 nm wavelength division multiplexer (WDM 1) is employed to couple the pump laser into the ring. An

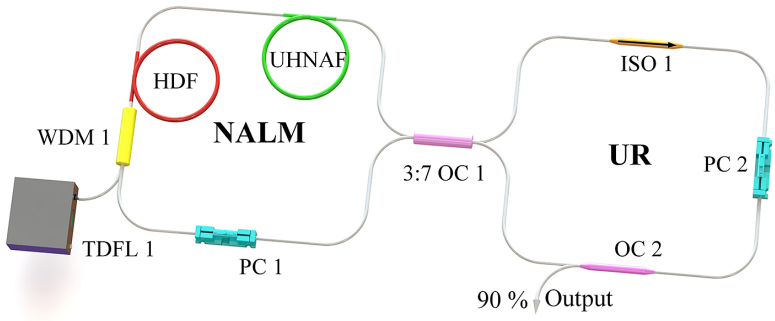

Figure 1. Experimental setup of the holmium-doped mode-locked seed laser.

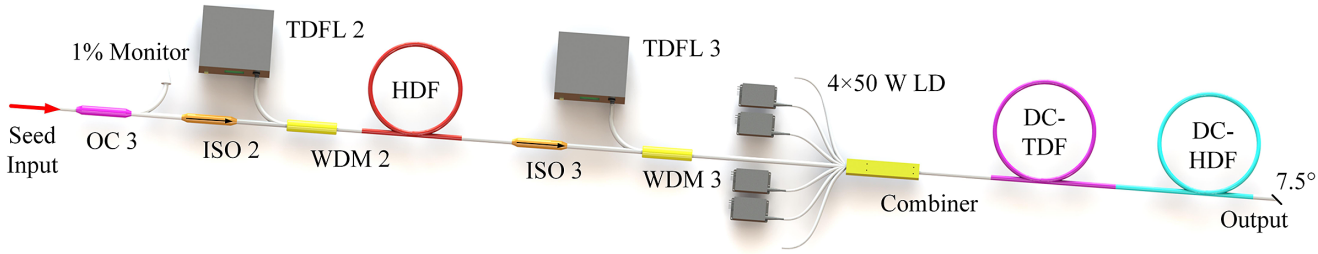

Figure 2. Schematic of the MOPA system.

8.5 m HDF with 8 μm core diameter and 0.2 numerical aperture (NA) is utilized as the gain medium. The intracavity dispersion is compensated by using ultra-high numerical aperture fiber (UHNAF, 2.2 μm core diameter and 0.35 NA) with an optimized length of 55 m. To enhance the nonlinear phase shift difference between clockwise and counter-clockwise propagating light in the NALM ring, the UHNAF is placed between the HDF and optical coupler (OC 1)[26]. The NALM ring is connected with the UR via the 2 × 2 3:7 OC 1. The use of asymmetric OC favors the enhancement of the nonlinear phase shift accumulation in the cavity[4]. In the UR, an isolator (ISO 1) is employed for ensuring unidirectional operation of the pulsed laser. The 90% port of the 10:90 OC 2 acts as the output of the seed laser and 10% port for cavity feedback. The change of the polarization states in the NALM ring and UR is achieved by adjusting the polarization controllers (PC 1 and PC 2, respectively). In the seed laser, the pigtail fibers of all fiber components are single-mode fiber (SMF). The SMF and HDF exhibit anomalous dispersion (–0.1 and –0.102 ps^2/m), while the UHNAF exhibits normal dispersion (+0.0815 ps^2/m) at 2.1 μm[27]. Considering the total cavity length of 75.5 m, the net dispersion in the cavity is calculated as +2.42 ps^2.

After the DSR mode-locked seed laser, OC 3 is used to monitor the seed pulses and ISO 2 is employed to protect the seed source, as shown in Figure 2. The first-stage amplifier consists of the 4.4 W CW TDFL 2, the 1950/2100 nm WDM 2, ISO 3 and a 2.8 m HDF. The parameters of the HDF used are identical to those in the seed laser. The second-stage amplifier is the main amplifier. A tandem pump layout with a 3.5 m double-clad TDF (DC-TDF, 25/250 μm core/cladding diameter and 0.09/0.46 NA) and a 3.6 m double-clad HDF (DC-HDF) is utilized. The DC-HDF has the same core/cladding diameter and NA as the DC-TDF. In this stage, the 4.5 W 1950 nm CW laser from TDFL 3 is efficiently amplified in the DC-TDF, while the 2100 nm signal from the pre-stage amplifier is amplified limitedly due to the low gain of the DC-TDF in the 2100 nm waveband. Then, the average power and pulse energy of the 2100 nm signal are scaled with high efficiency in the DC-HDF pumped by the 1950 nm CW light. The pump source is four 50 W 793 nm multimode laser diodes (LDs). A (6 + 1) × 1 combiner is employed to drive the 793 nm pump laser coupling into the gain fiber. A 0.7 m passive fiber matching the active fiber is spliced to the DC-HDF and the fiber end is cut at an angle of 7.5° to avoid back reflection. To enable excellent heat dissipation, the fibers in the second-stage amplifier are placed on a water-cooled plate.

The output characteristics of fiber laser system are measured by the following equipment: a real-time 2-GHz oscilloscope, a 12.5-GHz InGaAs photodetector, an optical spectrum analyzer with spectrum range of 1200–2400 nm, a radio-frequency (RF) spectrum analyzer with a 4 GHz bandwidth, an integrating sphere and an autocorrelator with a maximum scanning range of 50 ps.

3. Experimental results and discussion

3.1. Performance of the holmium-doped seed laser

Mode-locking is established by raising the TDFL 1 power to 3.8 W and tuning the PCs. The obtained pulse is able to be reproduced again when TDFL 1 is restarted. Figure 3(a) exhibits the evolution of the spectrum with enhancing TDFL 1 power. As the TDFL 1 power increases, the spectrum intensity increases and the 3-dB spectral bandwidth remains essentially unchanged. At the maximum TDFL 1 power, the center wavelength and 3-dB spectral bandwidth of the mode-locked pulse are 2103.7 and 0.48 nm, respectively. The pulse waveform versus pump power is depicted in Figure 3(b). The mode-locked pulse has a rectangular profile and the amplitude of the pulse is basically unchanged with increasing TDFL 1 power. Also, the pulse width is linearly increased from 10.2 to 17.1 ns.

At maximum TDFL 1 power of 5.1 W, the obtained pulse properties are as illustrated in Figure 4. The pulse sequence at approximately 4 μs is presented in Figure 4(a). The separation between adjacent pulses is 378.4 ns, consistent with the cavity round-trip time of the mode-locked pulse. The measured autocorrelation trace is plotted in Figure 4(b). No interference signal is detected within the scan range of 50 ps. Considering that the mode-locked pulse has a narrow spectrum as well as a rectangular waveform, there is a strong conviction that the pulses output from the seed laser are DSR pulses[28,29]. As shown in Figure 4(c), the

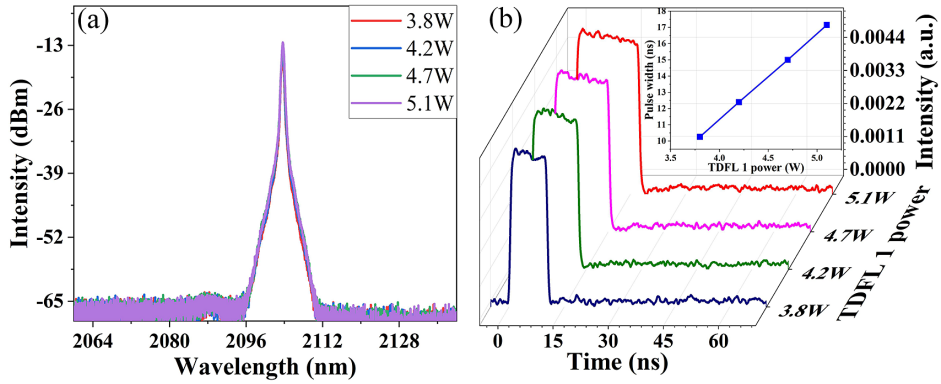

Figure 3. (a) The evolution of the optical spectrum with TDFL 1 power. (b) The waveforms under different TDFL 1 power levels. Inset: the pulse width dependence on TDFL 1 power.

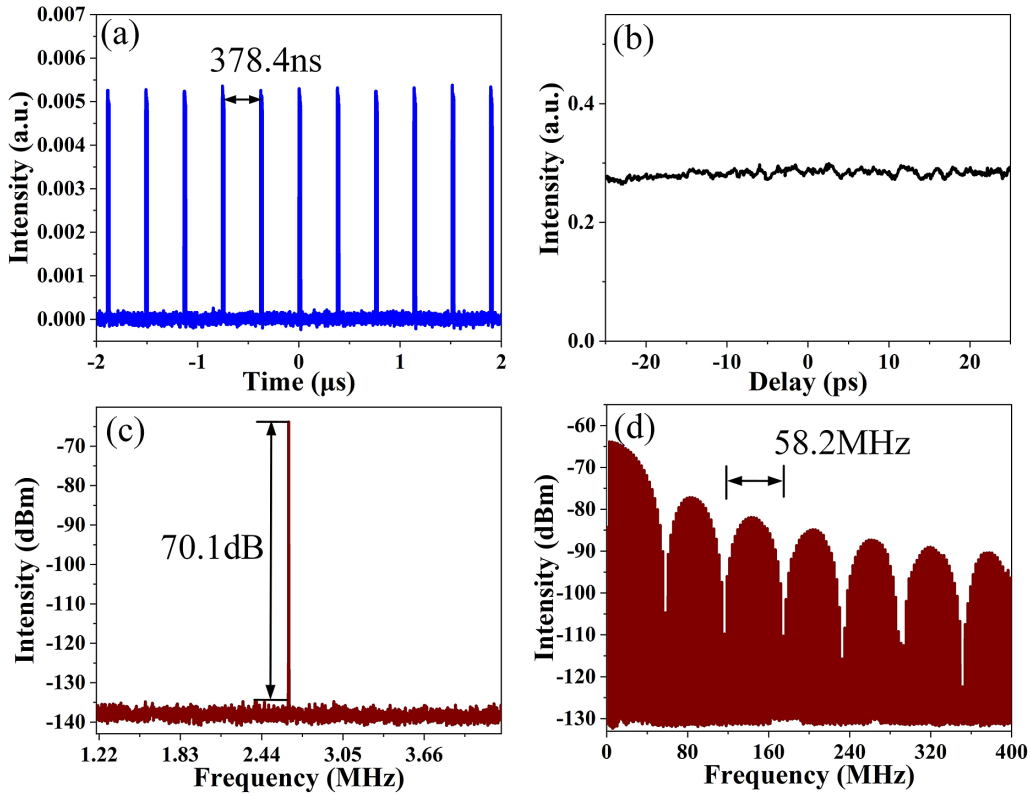

Figure 4. Mode-locked pulse properties. (a) Pulse sequence within approximately 4 μs. (b) Autocorrelation trace with 50 ps scan range. RF spectra measured at approximately (c) 2 MHz and (d) 400 MHz.

fundamental repetition frequency of the pulse is 2.643 MHz, matching the cavity length. The signal-to-noise ratio (SNR) is 70.1 dB. Figure 4(d) exhibits a wide scanning range of the RF spectrum with 100 Hz resolution, demonstrating the good stability of the DSR operation. Note that the periodic modulation envelope appears on the RF spectrum, showing that the modulation width is about 58.2 MHz, which is the inverse of the pulse width.

Figure 5(a) shows the evolutions of output power and pulse energy with TDFL 1 power. The output power of the seed laser increases monotonically from 0.154 to 0.233 W and the corresponding slope efficiency is 5.9%. The maximum pulse energy reaches 88.1 nJ. The obtained conversion efficiencies (defined as the output power divided by the pump power) at different TDFL 1 powers are shown in Figure 5(b). The conversion efficiency increases slightly to 4.57% with increasing TDFL 1 power to 5.1 W.

In the experiment, the use of different gain fiber lengths affects the center wavelength and output power of the obtained DSR laser. In fact, the wavelength tunable operations of DSR lasers in a certain range are available by adjusting the intracavity polarization state at different

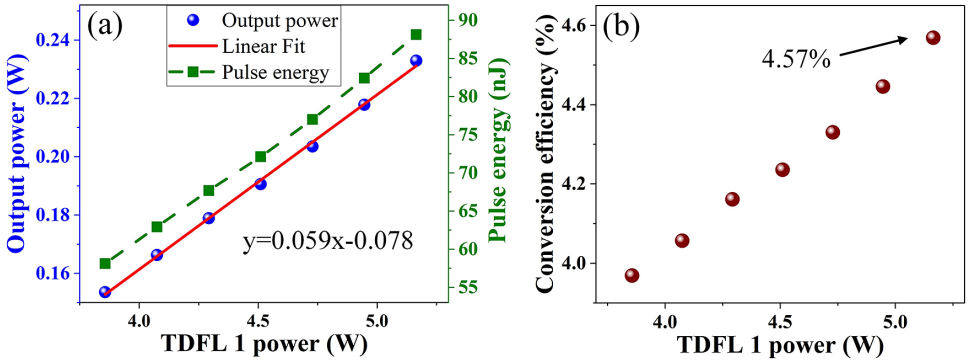

Figure 5. (a) Output power and pulse energy versus TDFL 1 power. (b) Conversion efficiency versus TDFL 1 power.

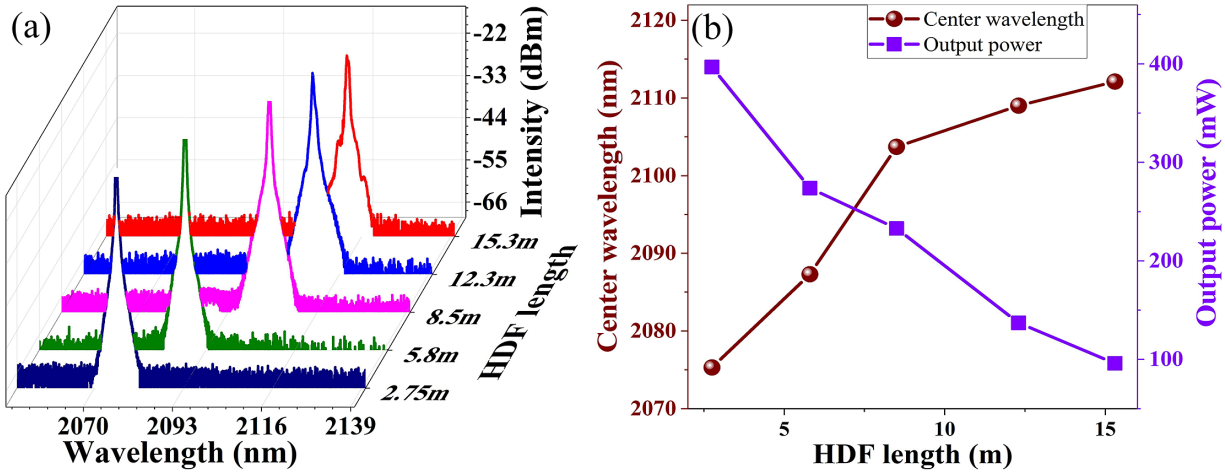

Figure 6. (a) Output spectra of mode-locked pulses under different HDF lengths. (b) Center wavelength and output power versus HDF length.

gain fiber lengths[30]. Taking into account that this work is targeted for the generation and amplification of DSR lasers, we plot the spectra of the obtained stable DSR lasers at the longest wavelength that can be adjusted for different HDF lengths, as shown in Figure 6(a). As the length of the HDF increases from 2.75 to 15.3 m, the center wavelength of the DSR pulse is redshifted from 2075.3 to 2112.1 nm. However, the output power gradually decreases from 396.7 to 96 mW due to the lower intracavity net gain at longer wavelengths. In this case, to obtain a DSR pulse at a wavelength exceeding 2.1 μm, we choose 8.5 m long HDF as the gain medium for the seed laser at the expense of output power.

The difference in net cavity dispersion directly affects the output characteristics of the mode-locking pulse. When the fiber laser is operated in the anomalous dispersion regime, a conventional soliton (CS) with Kelly sidebands is formed[31–33]. A dispersion managed soliton (DMS) and a dissipative soliton (DS) are achieved when increasing the net cavity dispersion to near zero dispersion and normal dispersion regimes[34,35]. For the CS, DMS and DS, it is difficult to obtain nanosecond width by designing the cavity structure, while with making the seed laser operate in the noise-like pulse (NLP) and DSR regimes, pulses with nanosecond width can be easily obtained. NLP is composed of many solitons with random amplitude and phase[36]. Therefore, NLP undergoes dramatic spectral broadening in high-power scaling due to strong nonlinear effects, which seriously affects the application of NLP in mid-infrared nonlinear frequency conversion. In contrast, DSR pulses operating in the normal dispersion regime have a narrow spectrum and wide pulse width (usually at the nanosecond level). The NALM-based figure-of-eight cavity structure has a long cavity configuration, which makes it easier to obtain pulses with nanosecond pulse width. Therefore, we design the net normal dispersion figure-of-eight fiber laser and use a piece of UHNAF to manage the intracavity dispersion. The pulse widths of the mode-locked pulse are different when the UHNAF is located at different positions in the cavity. To obtain DSR pulses with the largest pulse width, the UHNAF is placed between the HDF and OC 1. Since the pulse energy of a mode-locked fiber laser is dependent on the cavity length and output power, the UHNAF length is optimized to obtain the maximum pulse energy. The length of the UHNAF can be varied from 30 to 125 m with the corresponding intracavity net dispersion changing from +0.41 to +8.15 ps^2. When further shortening the UHNAF length to 11 m, the seed

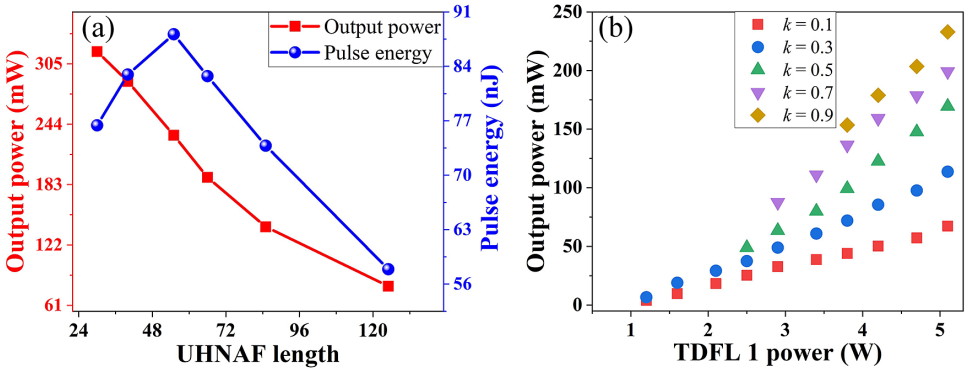

Figure 7. (a) Variations of output power and pulse energy of a seed laser with UHNAF length. (b) Variation of output power with increasing TDFL 1 power under different output coupling ratios (k).

Table 1. Summary of holmium-doped mode-locked DSR fiber lasers.

Center wavelength (nm)	Output power (W)	Pulse energy (nJ)	Conversion efficiency (%)	Reference
2024.2	0.0156	5.8	0.39	[23]
2050.373	0.0189	12.4	0.39	[38]
2045.3	0.0383	26.5	0.98	[25]
2076	0.01794	2	0.85	[24]
2103.7	0.233	88.1	4.57	This work

laser operates in the NLP regime. Increasing the UHNAF length to 140 m, only CW operation is observed because the intracavity loss is higher than the available gain. The variations of the output power and pulse energy as a function of the UHNAF length are presented in Figure 7(a). As the fiber length increases, the output power gradually decreases from 317.4 to 80.4 mW due to the increase in propagation loss of the pulsed laser and absorption loss of the saturable absorber[37]. As a result of the increase in cavity length, the repetition frequency of the DSR pulse decreases from 4.154 to 1.389 MHz. For pulse energy of the seed laser, when the influence of reduced output power is weaker than the influence of decreased repetition frequency, the pulse energy will gradually increase. Thus, with the increasing UHNAF length from 30 to 55 m, the pulse energy of the DSR pulse increases from 76.4 to 88.1 nJ. However, the pulse energy reduces to 57.9 nJ when increasing the length of UHNAF to 125 m, indicating that the reduced output power has a greater influence on the pulse energy. As a result, an 88.1 nJ DSR pulse is obtained at an optimized UHNAF length of 55 m.

In addition, an OC with a high output coupling ratio (k) as the output of the seed laser also benefits the achievement of high-energy DSR pulses. Figure 7(b) exhibits the evolution of the output power with the TDFL 1 power under different k values. At TDFL 1 power of 5.1 W, the output power of seed laser increases from 67.4 to 232.9 mW as the k value increases from 0.1 to 0.9. The corresponding pulse energy increases from 25.3 to 88.1 nJ. Although the threshold power required to achieve mode-locking grows as the k value increases, the use of long gain fiber combined with a strong pump condition ensures the establishment of mode-locking at 2.1 μm. On the other hand, the utilization of UHNAF has higher nonlinearity than SMF and an antisymmetric OC can introduce sufficient nonlinear phase shift difference in the seed laser, which reduces the mode-locking threshold power and enables the implementation of mode-locking with small intracavity feedback power.

We summarize the output characteristics of the holmium-doped mode-locked DSR fiber lasers in Table 1. One can see that we obtain the longest wavelength and the highest energy DSR pulse so far. The output power and conversion efficiency have an order of magnitude improvement compared with other work. This is attributed to our choice of an output coupler with a large coupling ratio as well as the optimization of the length of the intracavity dispersion compensation fiber. In our experiment, the average power of the obtained DSR pulse is only 21.3 mW when using an output coupler with a low coupling ratio ($k = 0.1$) and a long UHNAF (125 m). The corresponding pulse energy and conversion efficiency are 15.3 nJ and 0.41%, respectively. By shortening the length of the UHNAF to 55 m, the output power and conversion efficiency of the DSR pulse are improved to 67.4 mW and 1.32%, respectively, due to the reduced transmission loss in the fiber. With the increase of the k value to 0.9, a 0.233 W DSR pulse with a pulse energy of 88.1 nJ is finally obtained under maximum TDFL 1 power because more energy is extracted out of the cavity. The conversion efficiency reaches 4.57%. Further improvements in fiber laser performance require the use of passive fiber with lower transmission loss (e.g., SM1950) as the pigtails of fiber components as well as optimization of the OC 1 coupling ratio.

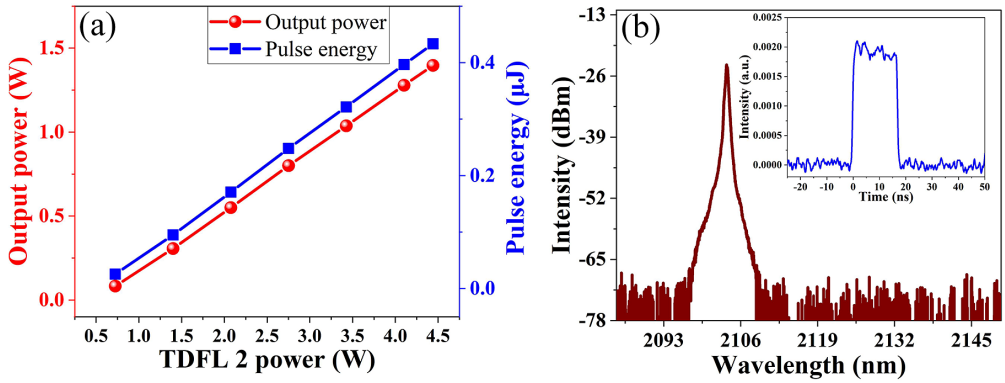

Figure 8. (a) Evolutions of output power and pulse energy as a function of TDFL 2 power. (b) Optical spectrum and waveform at the maximum power of TDFL 2.

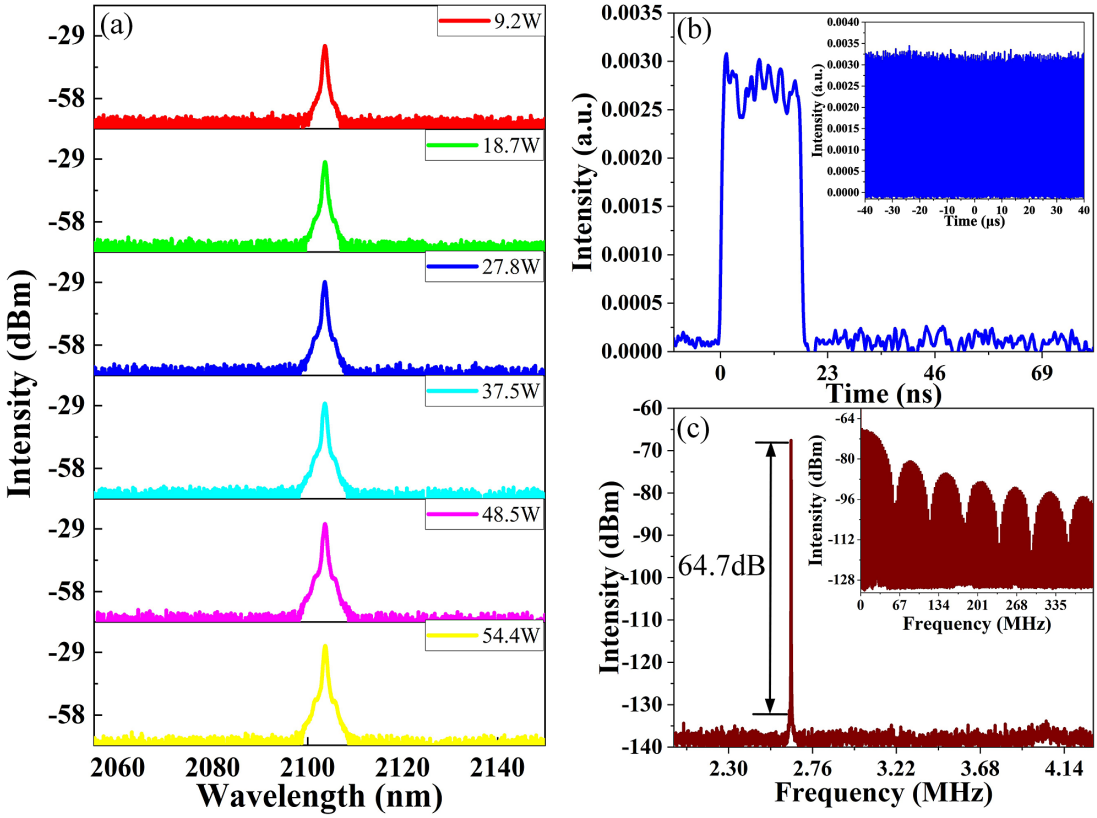

Figure 9. (a) Optical spectra versus output power. (b) Pulse envelope at maximum output power. Inset: pulse train at approximately 80 μs. (c) The RF spectrum captured under output power of 54.4 W. Inset: RF spectrum at approximately 400 MHz.

3.2. Output characteristics of the DSR amplification system

After the seed laser, the average power of the DSR pulse decreases to 101.2 mW before accessing the first-stage amplifier. The decrease in average power is attributed to the insert losses of OC 3 (1.92 dB) and ISO 2 (1.7 dB). In the first-stage amplifier, the 2103.7 nm DSR pulse is amplified by using the core pump scheme. Figure 8 shows the performance of the first-stage amplifier. The first-stage amplifier drives the average power and pulse energy of the DSR pulse to 1.39 W and 0.43 μJ, respectively. At the maximum power of TDFL 2, there is no significant change in the 3-dB spectral bandwidth and pulse duration compared to the seed laser, as shown in Figure 8(b).

Then, the average power and pulse energy of the DSR pulse are further boosted in the main amplifier. Figure 9(a) plots the DSR spectra at different output power levels. With the enhancement of output power from 9.2 to 54.4 W, the spectral intensity gradually increases and the 3-dB spectral bandwidth broadens slightly to 0.52 nm. No significant nonlinear effects are observed in the spectrum. Figure 9(b) records the pulse train at maximum output power of 54.4 W,

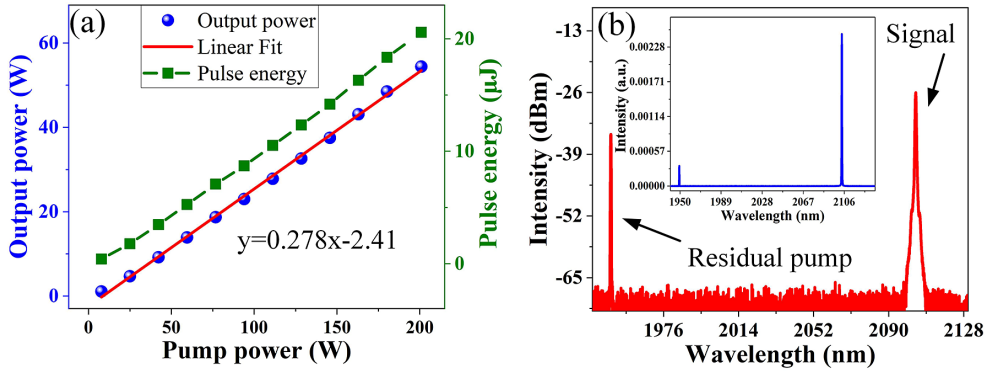

Figure 10. (a) Output power and pulse energy with increasing 793 nm pump power. (b) Optical spectra in logarithmic and linear coordinates with spectrum resolution of 0.05 nm at output power of 54.4 W.

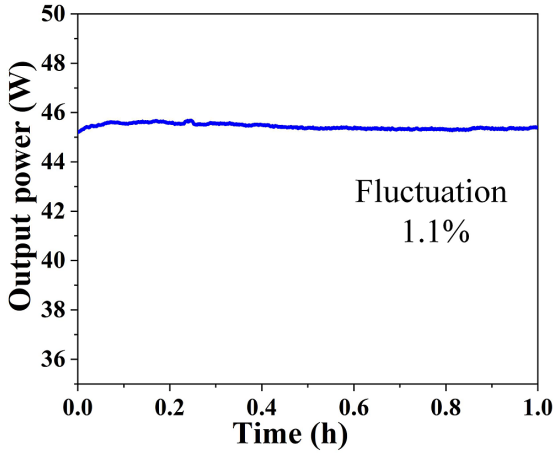

Figure 11. Measured power fluctuation over 1 hour under average output power of 45.4 W.

which indicates that there is no noticeable alteration in the pulse waveform. The time domain at approximately 80 μs shows the low-intensity fluctuation of the pulse train. The RF spectra of the amplified DSR pulses are measured as shown in Figure 9(c). Due to the amplification, the SNR of the DSR pulses slightly decreases from 70.1 to 64.7 dB. However, the wide range of the RF spectrum still exhibits high stability of the amplified DSR pulses, as presented in the inset of Figure 9(c).

As shown in Figure 10(a), the output power is linearly increased with the enhancement of pump power and the overall slope efficiency (from 793 nm pump power to output power) is 27.8%. Under the maximum pump power, the output power and pulse energy of the main amplifier reach 54.4 W and 20.58 μJ, respectively. Figure 10(b) records wide-range spectra in logarithmic and linear coordinates at the maximum output power level. The residual pump light component occupies 7.3% of the total spectrum component. Thus, the average power and pulse energy of the 2103.7 nm signal laser are calculated as 50.4 W and 19.1 μJ, respectively. During the amplification process, no power saturation phenomenon occurs. The power stability of the DSR laser system is checked as presented in Figure 11. The power fluctuation is 1.1% over 1 hour, indicating the good operating capability of the whole laser system. The performance comparison of holmium-doped mode-locked fiber laser systems so far is shown in Table 2. It can be seen that no high-power DSR system has been reported. The pulse energy of the DSR pulse we obtained is the highest pulse energy in a holmium-doped mode-locked fiber laser system. We think that further scaling of the DSR power could be achievable by raising the pump power and optimizing the gain fiber in the main amplifier.

4. Conclusion

In summary, we demonstrate a high-energy all-fiber holmium-doped laser system, operating in the DSR regime. The fiber laser system consists of a NALM mode-locked seed laser and dual-stage amplifiers. In the seed laser, we use a long gain fiber and in-band pump solution for efficient excitation at 2.1 μm. An optimized UHNAF with normal

Table 2. Performance comparison of holmium-doped mode-locked fiber laser systems.

System configuration	Pulse type	Output power (W)	Pulse energy (μJ)	Reference
SESAM [a] + single-stage amplifier	CS	2.08	0.076	[39]
NPR + single-stage amplifier	CS	~0.2	0.007	[40]
Hybrid mode-locking + single-stage amplifier	CS	0.4	0.02	[3]
NALM + single-stage amplifier	NLP	5.8	1.52	[37]
NALM + dual-stage amplifiers	DSR	50.4	19.1	This work

[a]SESAM: semiconductor saturable absorber mirror.

dispersion and high nonlinearity and an output coupler with a large coupling ratio are employed to obtain high-energy pulses. At the net cavity dispersion of $+2.42$ ps^2, a 0.233 W, 88.1 nJ DSR pulse centered at 2103.7 nm is obtained. The achieved mode-locked pulse has a pulse width of 17.1 ns and a 3-dB spectral bandwidth of 0.48 nm. The conversion efficiency reaches 4.57%. The output power and conversion efficiency are improved by an order of magnitude compared with previous holmium-doped DSR seed lasers. Benefiting from the high output power and nanosecond pulse width of the seed laser, the average power of the DSR pulse can be linearly boosted to 50.4 W with a dual-stage MOPA amplification system. The corresponding pulse energy reaches 19.1 μJ. The 3-dB spectral bandwidth slightly broadened to 0.52 nm and no distortion of the pulse waveform is observed. The power fluctuation measured over 1 hour is 1.1%, demonstrating the good stability of the fiber laser system. This work not only achieved the high-power amplification of 2.1 μm DSR pulses for the first time, but also obtained the highest output energy of 2.1 μm DSR pulses. The obtained 2.1 μm band, high-energy DSR pulse with relatively wide pulse width has excellent prospects for ZGP-based OPOs.

Acknowledgements

This work was supported by the State Key Laboratory of Pulsed Power Laser Technology, China (Nos. SKL2021KF07 and SKL2020ZR06) and the Postgraduate Scientific Research Innovation Project of Hunan Province, China (Nos. CX2022078 and CX2022080). The authors are grateful to Sen Guo and Weide Hong for their assistance during the experiment.

References

1. P. Lin, T. Wang, W. Ma, Q. Yang, and Z. Liu, Opt. Express **28**, 39216 (2020).
2. J. Le Gouët, F. Gustave, P. Bourdon, T. Robin, A. Laurent, and B. Cadier, Opt. Express **28**, 22307 (2020).
3. M. S. Kopyeva, S. A. Filatova, V. A. Kamynin, A. I. Trikshev, E. I. Kozlikina, V. V. Astashov, V. B. Loschenov, and V. B. Tsvetkov, Appl. Sci. **12**, 3825 (2022).
4. J. Wang, J. Han, J. He, C. Liao, and Y. Wang, Opt. Lett. **44**, 4491 (2019).
5. M. A. Medina, M. Piotrowski, M. Schellhorn, F. R. Wagner, A. Berrou, and A. Hildenbrand-Dhollande, Opt. Express **29**, 21727 (2021).
6. J. Yuan, C. Li, B. Yao, J. Yao, X. Duan, Y. Li, Y. Shen, Y. Wu, Z. Cui, and T. Dai, Opt. Express **24**, 6083 (2016).
7. L. G. Holmen and H. Fonnum, Opt. Express **29**, 8477 (2021).
8. C. Kieleck, A. Berrou, B. Donelan, B. Cadier, T. Robin, and M. Eichhorn, Opt. Lett. **40**, 1101 (2015).
9. M. Gebhardt, C. Gaida, P. Kadwani, A. Sincore, N. Gehlich, C. Jeon, L. Shah, and M. Richardson, Opt. Lett. **39**, 1212 (2014).
10. J. Shang, S. Zhao, Y. Liu, Y. Zhao, Y. Song, T. Li, and T. Feng, J. Lightwave Technol. **40**, 2116 (2022).
11. M. Bartnick, G. Bharathan, T. A. Goebel, R. G. Krämer, S. Nolte, and C.-S. Brès, Opt. Lett. **47**, 2085 (2022).
12. N. Dalloz, T. Robin, B. Cadier, C. Kieleck, M. Eichhorn, and A. Hildenbrand-Dhollande, Opt. Express **27**, 8387 (2019).
13. W. Yao, C. Shen, Z. Shao, Q. Liu, H. Wang, Y. Zhao, and D. Shen, Opt. Express **26**, 8841 (2018).
14. C. Mahnke, Y. Hua, Y. Ma, S. Salman, T. Lamb, S. Schulz, C. M. Heyl, H. Cankaya, and I. Hartl, Opt. Lett. **47**, 822 (2022).
15. J. Wang, D. I. Yeom, N. Simakov, A. Hemming, A. Carter, S. B. Lee, and K. Lee, J. Lightwave Technol. **36**, 5863 (2018).
16. W. Chang, A. Ankiewicz, J. M. Soto-Crespo, and N. Akhmediev, Phys. Rev. A **78**, 023830 (2008).
17. J. Li, C. Wang, and P. Wang, J. Lightwave Technol. **40**, 5958 (2022).
18. Z. Wang and W. Wu, Opt. Laser Technol. **133**, 106503 (2021).
19. S. Liu, P. Guo, X. He, Z. Dou, D. Zhao, L. Yang, B. Zhang, and J. Hou, Opt. Express **30**, 4592 (2022).
20. D. Mao, X. Liu, L. Wang, H. Lu, and H. Feng, Opt. Express **18**, 23024 (2010).
21. L. Wang, J. Xu, J. Lu, L. Teng, Z. Luo, F. Pang, and X. Zeng, Nanophotonics **10**, 3527 (2021).
22. Z. Zheng, D. Ouyang, X. Ren, J. Wang, J. Pei, and S. Ruan, Photonics Res. **7**, 513 (2019).
23. J. Zhao, L. Li, L. Zhao, D. Tang, and D. Shen, IEEE Photonics Technol. Lett. **30**, 1699 (2018).
24. X. Li, T. Wang, W. Ma, L. Du, H. Ren, and L. Xiao, IEEE Photonics J. **14**, 1546104 (2022).
25. J. Zhao, J. Zhou, Y. Jiang, L. Li, D. Shen, A. Komarov, L. Su, D. Tang, M. Klimczak, and L. Zhao, J. Lightwave Technol. **38**, 6069 (2020).
26. Z. Guo, Q. Hao, J. Peng, and H. Zeng, High Power Laser Sci. Eng. **7**, e47 (2019).
27. M. Pawliszewska, A. Duzynska, M. Zdrojek, and J. Sotor, Opt. Lett. **45**, 956 (2020).
28. W. Stepien and J. R. Marciante, J. Opt. Soc. Am. B **39**, 626 (2022).
29. C. Shang, X. Li, Z. Yang, S. Zhang, M. Han, and J. Liu, J. Lightwave Technol. **36**, 4932 (2018).
30. B. Posada-Ramírez, M. Durán-Sánchez, R. I. Álvarez-Tamayo, B. Ibarra-Escamilla, E. Bravo-Huerta, and E. A. Kuzin, Opt. Express **25**, 2560 (2017).
31. S. Kelly, in *International Quantum Electronics Conference* (Optica Publishing Group, 1992), paper TuH3.
32. Y. Wang, S. Fu, C. Zhang, X. Tang, J. Kong, J. H. Lee, and L. Zhao, J. Lightwave Technol. **39**, 2542 (2021).
33. Y. Wang, S. Fu, J. Kong, A. Komarov, M. Klimczak, R. Buczyński, X. Tang, M. Tang, Y. Qin, and L. Zhao, Photonics Res. **9**, 1531 (2021).
34. H. Chi, B. Liu, Y. Song, M. Hu, L. Chai, W. Shen, X. Liu, and C. Wang, High Power Laser Sci. Eng. **6**, e27 (2018).
35. F. Ilday, F. Wise, and T. Sosnowski, Opt. Lett. **27**, 1531 (2002).
36. H. Santiago-Hernandez, O. Pottiez, M. Duran-Sanchez, R. I. Alvarez-Tamayo, J. P. Lauterio-Cruz, J. C. Hernandez-Garcia, B. Ibarra-Escamilla, and E. A. Kuzin, Opt. Express **23**, 18840 (2015).
37. D. Zhao, B. Zhang, X. Zhu, S. Liu, L. Yang, and J. Hou, Opt. Express **30**, 3601 (2022).
38. J. Zhao, J. Zhou, L. Li, L. Zhao, D. Tang, D. Shen, and L. Su, Opt. Lett. **44**, 2414 (2019).
39. M. Hinkelmann, D. Wandt, U. Morgner, J. Neumann, and D. Kracht, Opt. Express **25**, 20522 (2017).
40. M. Wang, H. Zhang, R. Wei, Z. Zhu, S. Ruan, P. Yan, J. Wang, T. Hasan, and Z. Sun, Opt. Lett. **43**, 4619 (2018).